Anomalous quartic $ZZ\gamma\gamma$ couplings in γp collision at the LHC

İ. Şahin* and B. Şahin†

Department of Physics, Bulent Ecevit University, 67100 Zonguldak, Turkey

Abstract

We investigate the constraints on the anomalous quartic $ZZ\gamma\gamma$ couplings through the process $pp \to p\gamma p \to p\gamma qZX$ at the LHC. Taking into consideration various forward detector acceptances and integrated LHC luminosities, we find 95% confidence level bounds on the anomalous coupling parameters. We show that the bounds on these couplings are at the order of 10^{-6} GeV^{-2} which are about four orders of magnitude more restricted with respect to current experimental bounds.

*inancsahin@karaelmas.edu.tr

†bsahin@karaelmas.edu.tr

I. INTRODUCTION

Precision measurements of gauge boson self-interactions at the LHC will be the crucial test of the $SU_L(2)\times U_Y(1)$ gauge structure of the standard model (SM). Any deviation of the couplings from the SM expectations would indicate the existence of new physics. It is very common to investigate the new physics via effective Lagrangian approach. The theoretical basis of such an approach rely on the assumption that at higher energies beyond the SM, there is a more fundamental theory which reduces to the SM at lower energies. Hence, SM is assumed to be an effective low-energy theory in which heavy fields have been integrated out. Such a procedure is quite general and independent of the details of the model. For this reason this approach is sometimes called model independent analysis.

In this paper we have analyzed genuine quartic $ZZ\gamma\gamma$ couplings via single Z boson production in a γ-proton collision at the LHC. Genuine quartic couplings have different origins than anomalous trilinear couplings. They arise from effective operators that do not induce any trilinear gauge boson coupling. Hence, genuine quartic couplings are free from constraints on trilinear couplings. Imposing custodial $SU(2)_{Weak}$ symmetry and local $U(1)_{em}$ symmetry, C and P conserving dimension 6 effective lagrangian for $ZZ\gamma\gamma$ couplings are given by [1–3],

$$\mathcal{L} = \mathcal{L}_0 + \mathcal{L}_c \tag{1}$$

$$\mathcal{L}_0 = \frac{-\pi\alpha}{4\Lambda^2} a_0 F_{\mu\nu} F^{\mu\nu} W^{(i)}_{\alpha} W^{(i)\alpha} \tag{2}$$

$$\mathcal{L}_c = \frac{-\pi\alpha}{4\Lambda^2} a_c F_{\mu\alpha} F^{\mu\beta} W^{(i)\alpha} W^{(i)}_{\beta} \tag{3}$$

where $W^{(i)}$ is the $SU(2)_{Weak}$ triplet, and $F_{\mu\nu}$ is the electromagnetic field strength. a_0 and a_c are the dimensionless anomalous coupling constants and Λ is the scale of new physics. The vertex functions generated from the effective lagrangians (2) and (3) are given respectively by [3]

$$i\frac{2\pi\alpha}{\cos^2\theta_W \Lambda^2} a_0 g_{\mu\nu} \left[g_{\alpha\beta}(p_1.p_2) - p_{2\alpha} p_{1\beta}\right] \tag{4}$$

$$\begin{aligned} i\frac{\pi\alpha}{2\cos^2\theta_W \Lambda^2} a_c \big[&(p_1.p_2)(g_{\mu\alpha}g_{\nu\beta} + g_{\mu\beta}g_{\alpha\nu}) + g_{\alpha\beta}(p_{1\mu}p_{2\nu} + p_{2\mu}p_{1\nu}) \\ &- p_{1\beta}(g_{\alpha\mu}p_{2\nu} + g_{\alpha\nu}p_{2\mu}) - p_{2\alpha}(g_{\beta\mu}p_{1\nu} + g_{\beta\nu}p_{1\mu})\big] \end{aligned} \tag{5}$$

where p_1 and p_2 are the momenta of photons and for a convention, we assume that all the momenta are incoming to the vertex.

The current best limits on $ZZ\gamma\gamma$ couplings are provided by the OPAL Collaboration. These are

$$-0.007 \text{ GeV}^{-2} < \frac{a_0}{\Lambda^2} < 0.023 \text{ GeV}^{-2} \tag{6}$$

$$-0.029 \text{ GeV}^{-2} < \frac{a_c}{\Lambda^2} < 0.029 \text{ GeV}^{-2} \tag{7}$$

at 95% C.L. [4].

Studying photon-induced reactions in a hadron collider is not a very new phenomena. The reactions such as $p\bar{p} \to p\gamma\gamma\bar{p} \to pe^+e^-\bar{p}$ [5, 6], $p\bar{p} \to p\gamma\gamma\bar{p} \to p\ \mu^+\mu^-\bar{p}$ [6, 7], $p\bar{p} \to p\gamma\bar{p} \to p\ J/\psi\ (\psi(2S))\bar{p}$ [7] were verified experimentally by the CDF collaboration at the Fermilab Tevatron. These results raise interest on the potential of LHC as a photon-photon and photon-proton collider. Probing new physics via photon-induced reactions at the LHC is common in the literature. Phenomenological studies involve: supersymmetry, extradimensions, unparticle physics, gauge boson self-interactions, neutrino electromagnetic properties etc. [8–22].

II. EQUIVALENT PHOTON APPROXIMATION AND CROSS SECTIONS

A quasireal photon emitted from one proton beam can interact with the quarks of the other proton and the subprocess $\gamma q \to \gamma qZ$ can occur at the LHC. Emitted quasireal photons are described by equivalent photon approximation (EPA) [23–25]. Their virtuality is very low and it is a good approximation to assume that they are on-mass-shell. Therefore to some extent it is possible to study γ-proton collision at the LHC. A schematic diagram describing this process is given in Fig.1.

Any process in a γ-proton collision can be discerned from pure deep inelastic scattering processes by means of two experimental signatures [26]: First signature is the forward large-rapidity gap. Quasireal photons have a low virtuality and scattered with small angles from the beam pipe. Since the transverse momentum carried by a quasireal photon is small, photon emitting intact protons should also be scattered with small angles and exit the central detector without being detected. This causes a decrease in the energy deposit in the corresponding forward region compared to the case in which the proton remnants are

detected by the calorimeters. As a result of this, one of the forward regions of the central detector has a significant lack of energy. This defines the forward large-rapidity gap and usual pp deep inelastic processes can be rejected by applying a selection cut on this quantity. Second experimental signature is provided by the forward detectors. Forward detectors are capable to detect particles with a large pseudorapidity. When a photon emitting intact proton is scattered with a large pseudorapidity, it exceeds the pseudorapidity coverage of the central detectors. The detection of this intact proton by the forward detectors provides a distinctive signal for the γ-proton collision.

$\gamma\gamma$ collision can also be studied in the framework of EPA. In fact, these two-photon processes are much more studied at the LHC. Two-photon processes provide a more clean environment with respect to γ-proton processes due to absence of the remnants of both proton beams. Moreover two-photon processes are generally electroweak in nature and they are mostly free from backgrounds coming from strong interactions. It is more probable for strong interactions that take part in a γ-proton process rather than in a two-photon process. Hence, two-photon processes generally have less backgrounds compared to γ-proton processes. On the other hand, for γ-proton processes energy reach and effective luminosity are much higher than for two-photon processes [26, 27]. This feature might be important in probing new physics especially when the energy dependences of the anomalous cross sections are very high. For instance, anomalous $ZZ\gamma\gamma$ couplings are described by effective lagrangians (2) and (3) which have an energy dimension of 6. Therefore anomalous cross section containing the $ZZ\gamma\gamma$ vertex has a higher momentum dependence than the SM cross section. From a simple dimensional analysis we deduce that its momentum dependence is higher up to a factor of p^4 than the SM cross section where p is the momentum incoming (or outgoing) to the vertex. Thus, new physics contribution to the cross section rapidly increases when the center-of-mass energy increases and the processes which have a higher energy reach are expected to have a high sensitivity to new physics. Another factor which has to be considered in a γ-proton or a $\gamma\gamma$ collision is the survival probability. It is basically defined as the probability of the scattered protons not to dissociate due to the secondary soft interactions [27]. In the γ-proton collision with quasireal photons virtuality of photons is very small. In the EPA that we have considered typical photon virtuality is $\langle Q^2 \rangle \approx 0.01 GeV^2$ [25]. Therefore proton impact parameter is much bigger than the range of strong interactions and proton survival probability is expected to be large. On the other hand, the survival

probability for a γ-proton process is usually smaller than for a two-photon process [27].

ATLAS and CMS collaborations have a program of forward physics with extra detectors located at distances of 220m and 420m from the interaction point [28, 29]. These forward detectors have a capability to detect intact scattered protons with momentum fraction loss in the interval $\xi_{min} < \xi < \xi_{max}$ which is called the acceptance of the forward detectors. The acceptance proposed by the ATLAS Forward Physics (AFP) Collaboration is $0.0015 < \xi < 0.15$ [28, 29]. The acceptance of the forward detectors in CMS is similar. There are also other scenarios with different acceptances. CMS-TOTEM forward detector scenario spans $0.0015 < \xi < 0.5$ [8, 30].

The process $\gamma q \to \gamma q Z$ takes part as a subprocess in the main reaction $pp \to p\gamma p \to p\gamma q Z X$. We consider totaly 10 subprocesses for different type of quarks and anti-quarks:

$$\begin{array}{ll} \text{(i)}\ \ \gamma u \to \gamma u Z & \text{(vi)}\ \ \gamma \bar{u} \to \gamma \bar{u} Z \\ \text{(ii)}\ \ \gamma d \to \gamma d Z & \text{(vii)}\ \ \gamma \bar{d} \to \gamma \bar{d} Z \\ \text{(iii)}\ \ \gamma c \to \gamma c Z & \text{(viii)}\ \ \gamma \bar{c} \to \gamma \bar{c} Z \\ \text{(iv)}\ \ \gamma s \to \gamma s Z & \text{(ix)}\ \ \gamma \bar{s} \to \gamma \bar{s} Z \\ \text{(v)}\ \ \gamma b \to \gamma b Z & \text{(x)}\ \ \gamma \bar{b} \to \gamma \bar{b} Z \end{array} \tag{8}$$

Each of the subprocesses is described by seven tree-level diagrams(Fig.2). We see from Fig.2 that one of them contains anomalous $ZZ\gamma\gamma$ vertex and others are SM contributions. The cross section for the main process $pp \to p\gamma p \to p\gamma q Z X$ can be obtained by integrating the cross sections for the subprocesses over the photon and quark spectra:

$$\begin{aligned} \sigma\left(pp \to p\gamma p \to p\gamma q Z X\right) &= \sum_q \int_{x_{1\,min}}^{x_{1\,max}} dx_1 \int_0^1 dx_2 \left(\frac{dN_\gamma}{dx_1}\right)\left(\frac{dN_q}{dx_2}\right) \hat{\sigma}_{\gamma q \to \gamma q Z}(\hat{s}) \\ &= \sum_q \int_{\frac{M_{inv}}{\sqrt{s}}}^{\sqrt{\xi_{max}}} dz\ 2z \int_{MAX(z^2,\xi_{min})}^{\xi_{max}} \frac{dx_1}{x_1}\left(\frac{dN_\gamma}{dx_1}\right) N_q(z^2/x_1)\ \hat{\sigma}_{\gamma q \to \gamma q Z}(z^2 s) \end{aligned} \tag{9}$$

where x_1 is the fraction which represents the ratio between the scattered equivalent photon and initial proton energy and x_2 is the momentum fraction of the proton's momentum carried by the quark. $\frac{dN_\gamma}{dx_1}$ is the equivalent photon spectrum (see Appendix) and $\frac{dN_q}{dx_2}$ is the quark distribution function of the proton. The summations in (9) are performed over subprocesses in (8). The second integral in (9) is obtained by transforming the differentials $dx_1 dx_2$ into $dz dx_1$ with a Jacobian determinant $2z/x_1$ where $z = \sqrt{x_1 x_2} \simeq \sqrt{\hat{s}/s}$. M_{inv} is the total

mass of the final particles of the subprocess $\gamma q \to \gamma q Z$. $N_q(z^2/x_1)$ is $\frac{dN_q}{dx_2}$ evaluated at $x_2 = z^2/x_1$. At high energies greater than proton mass, $\xi \simeq x_1$ holds. Therefore it is a good approximation to assume that $x_{1\,max} = \xi_{max}$ and $x_{1\,min} = \xi_{min}$ in the first integral in (9). During calculations, the virtuality of the quark is taken to be $Q^2 = {m_Z}^2$ where m_Z is the mass of the Z boson. In our calculations parton distribution functions of Martin, Stirling, Thorne and Watt [31] have been used.

In Figs.3 and 4 we plot the total cross section of the process $pp \to p\gamma p \to p\gamma qZX$ as a function of anomalous couplings $\frac{a_0}{\Lambda^2}$ and $\frac{a_c}{\Lambda^2}$ for the acceptances of $0.0015 < \xi < 0.5$ and $0.0015 < \xi < 0.15$. We observe from these figures that cross sections are large for $0.0015 < \xi < 0.5$ compared with $0.0015 < \xi < 0.15$ as expected. We also see from these figures that, deviation of the anomalous cross section from its SM value is larger for the coupling $\frac{a_0}{\Lambda^2}$ than $\frac{a_c}{\Lambda^2}$. Therefore sensitivity limits on the coupling $\frac{a_0}{\Lambda^2}$ are expected to be more restricted than the limits on $\frac{a_c}{\Lambda^2}$.

In all results presented in this paper we assume that center-of-mass energy of the proton-proton system is $\sqrt{s} = 14$ TeV and cross sections have evaluated numerically by a computer code GRACE [32].

III. LIMITS ON THE ANOMALOUS COUPLINGS

During statistical analysis we use two different method. We employ a simple one-parameter χ^2 test when the number of SM events is greater than 10. On the other hand, we employ a Poisson distribution when the number of SM events is less than or equal to 10. For AFP and CMS-TOTEM scenarios SM cross sections for the main reaction $pp \to p\gamma p \to p\gamma qZX$ are 0.0046 pb and 0.0047 pb respectively. Hence, the number of SM events exceeds 10 for integrated luminosities which are equal or greater than $100 fb^{-1}$. Therefore for AFP and CMS-TOTEM scenarios we employ both type of the statistical analysis depending on the luminosity. Forward detectors have a capability to detect protons in a continuous range of ξ. Therefore one can impose some cuts and choose to work in a subinterval of the whole acceptance region. Imposing such cuts on forward detector acceptance is useful in suppressing the SM contribution. In addition to AFP and CMS-TOTEM scenarios we will consider $0.1 < \xi < 0.15$ and $0.1 < \xi < 0.5$ subintervals of the whole AFP and CMS-TOTEM acceptance regions. For these acceptances the number of SM events is

less than 10. Therefore it is very appropriate to set bounds on the couplings using a Poisson distribution.

For the acceptances of $0.0015 < \xi < 0.5$ and $0.0015 < \xi < 0.15$ with a high luminosity, χ^2 analysis is performed. The χ^2 function is defined by

$$\chi^2 = \left(\frac{\sigma_{SM} - \sigma_{AN}}{\sigma_{SM}\ \delta} \right)^2 \tag{10}$$

where σ_{AN} is the cross section containing new physics effects and $\delta = \frac{1}{\sqrt{N}}$ is the statistical error. The expected number of events has been calculated considering the leptonic decay channel of the Z boson as the signal $N = S \times E \times \sigma_{SM} \times L_{int} \times BR(Z \to \ell\bar{\ell})$, where $\ell = e^-$ or μ^-, L_{int} is the integrated luminosity, E is the jet reconstruction efficiency and S is the survival probability factor. We have taken into account a jet reconstruction efficiency of $E = 0.6$ and survival probability factor of $S = 0.7$. This survival probability factor was proposed for the single W boson photoproduction [27, 33]. We assume that same survival factor is valid for our process. ATLAS and CMS have central detectors with a pseudorapidity coverage $|\eta| < 2.5$. Therefore we place a cut of $|\eta| < 2.5$ for final state particles. Moreover, we also demand that the transverse momenta of the final state photon and quark are greater than 15 GeV. For the acceptances of $0.1 < \xi < 0.15$ and $0.1 < \xi < 0.5$, we employ a Poisson distribution. Sensitivity limits are obtained assuming the number of observed events equal to the SM prediction, i.e., $N_{obs} = S \times E \times \sigma_{SM} \times L_{int} \times BR(Z \to \ell\bar{\ell})$. Upper limits of number of events N_{up} at the 95% C.L. can be calculated from the formula [27, 34]

$$\sum_{k=0}^{N_{obs}} P_{Poisson}(N_{up}; k) = 0.05 \tag{11}$$

Depending on the number of observed events, values for upper limits N_{up} can be found in Table 33.3 in Ref.[35]. In Table I we present number of observed events and upper limits of number of events for the cases in which the Poisson distribution has been used. In Table I the calculated N_{obs} values are rounded to the nearest integer. For instance, for forward detector acceptance of $0.1 < \xi < 0.5$, $N_{obs} = 0.69$ and 1.38 for $L_{int} = 100 fb^{-1}$ and $200 fb^{-1}$ respectively. Both of the N_{obs} values have been rounded to 1. The upper limits of number of events N_{up} can be directly converted to the limits of anomalous couplings $\frac{a_0}{\Lambda^2}$ and $\frac{a_c}{\Lambda^2}$. In Tables II and III, we show 95% C.L. sensitivity limits on the anomalous couplings $\frac{a_0}{\Lambda^2}$ and $\frac{a_c}{\Lambda^2}$ for various integrated luminosities and forward detector acceptances of $0.0015 < \xi < 0.5$, $0.1 < \xi < 0.5$, $0.0015 < \xi < 0.15$ and $0.1 < \xi < 0.15$. We see from Tables II and III that

our limits are at the order of 10^{-6} GeV^{-2} and limits on the coupling $\frac{a_0}{\Lambda^2}$ are more restricted than the limits on $\frac{a_c}{\Lambda^2}$.

In this paper we considered all tree-level SM contributions for the subprocess $\gamma q \to \gamma q Z$ (Fig.2). These constitute major SM contributions. Any other SM contribution coming to this subprocess is at the loop level and can be neglected compared to tree-level SM contributions. The leading order background process might be the pomeron exchange. A pomeron emitted from one proton beam can interact with the quarks of the other proton and same final state can occur. But when we analyze in detail we see that this background process is expected to has a minor influence on sensitivity bounds. In the deep inelastic scattering the virtuality of the struck quark is very high. During calculations in this paper, the virtuality of the struck quark is taken to be $Q^2 = {m_Z}^2$ where m_Z is the mass of the Z boson. Therefore, when a pomeron strikes a quark it probably dissociates into partons. These pomeron remnants can be detected by the calorimeters and background from pomeron exchange can be eliminated. Furthermore, survival probability for a pomeron exchange is considerably smaller than that for a photon exchange. Hence, even if the background from pomeron exchange can not be eliminated, it can not be much bigger (probably smaller) than the tree-level SM contributions for the photon exchange. Finally we would like to stress that our bounds are not very sensitive to backgrounds. For instance, if we assume that background cross section is 2 times bigger than the tree-level SM contributions, our limits with a $200 fb^{-1}$ luminosity are spoiled approximately a factor of 1.5 for $0.1 < \xi < 0.5$ and a factor of 1.3 for $0.0015 < \xi < 0.5$.

IV. CONCLUSIONS

The process $pp \to p\gamma p \to p\gamma q Z X$ at the LHC with a center-of-mass energy of 14 TeV probes anomalous quartic $ZZ\gamma\gamma$ couplings with a far better sensitivity than the current experimental bounds. It allows to improve the current sensitivity by almost four orders of magnitude. The potential of LHC to probe anomalous quartic $ZZ\gamma\gamma$ couplings was examined via weak boson fusion processes $qq \to qq\gamma\gamma$ and $qq \to qq\gamma Z(\to l^+l^-)$ [36] and photon-photon fusion process $pp \to p\gamma\gamma p \to pZZp$ [12, 21, 27, 34]. In papers [27, 34] authors considered semi-leptonic decay channel of the final Z bosons ,i.e., $ZZ \to \ell^+\ell^- jj$ where j refers to jets. On the other hand in papers [12, 21] authors considered fully-leptonic decay channel of the

final Z bosons. The bounds obtained in [12, 21] are considerably weaker than the bounds obtained in papers [27, 34]. This probably originates from the fact that semi-leptonic decay channel of the final Z bosons has a large branching ratio compared to fully-leptonic decay channel. In our paper we have considered leptonic decay channel of final Z. Therefore it is more appropriate to compare our bounds with the bounds obtained in [12, 21]. The bounds obtained in [12, 21, 36] are of the same order as our bounds. Anomalous quartic $ZZ\gamma\gamma$ couplings were also studied for future International Linear Collider (ILC) and its operating modes of $e\gamma$ and $\gamma\gamma$. The limits expected to be obtained for such a machine are comparable with the LHC bounds [37].

Appendix: Equivalent Photon Spectrum

Taking into consideration the electromagnetic form factors of the proton, equivalent photon spectrum of virtuality Q^2 and energy E_γ is given by the following formula [23–25]

$$\frac{dN_\gamma}{dE_\gamma dQ^2} = \frac{\alpha}{\pi}\frac{1}{E_\gamma Q^2}[(1-\frac{E_\gamma}{E})(1-\frac{Q^2_{min}}{Q^2})F_E + \frac{E_\gamma^2}{2E^2}F_M] \tag{A.1}$$

where

$$Q^2_{min} = \frac{m_p^2 E_\gamma^2}{E(E-E_\gamma)}, \quad F_E = \frac{4m_p^2 G_E^2 + Q^2 G_M^2}{4m_p^2 + Q^2} \tag{A.2}$$

$$G_E^2 = \frac{G_M^2}{\mu_p^2} = (1+\frac{Q^2}{Q_0^2})^{-4}, \quad F_M = G_M^2, \quad Q_0^2 = 0.71\text{GeV}^2 \tag{A.3}$$

In the above formula, E is the energy of the incoming proton beam and m_p is the mass of the proton. F_E and F_M are functions of the electric and magnetic form factors. μ_p^2 is the magnetic moment of the proton. It is taken to be $\mu_p^2 = 7.78$. dQ^2 integration in (A.1) can be easily performed analytically. After integration over Q^2, (A.1) takes the form of [8]

$$\frac{dN_\gamma}{dE_\gamma} = \frac{\alpha}{\pi E_\gamma}\left(1-\frac{E_\gamma}{E}\right)\left[\varphi\left(\frac{Q^2_{max}}{Q_0^2}\right) - \varphi\left(\frac{Q^2_{min}}{Q_0^2}\right)\right] \tag{A.4}$$

where the function φ is defined by

$$\varphi(x) = (1+ay)\left[-ln(1+\frac{1}{x}) + \sum_{k=1}^{3}\frac{1}{k(1+x)^k}\right] + \frac{y(1-b)}{4x(1+x)^3}$$
$$+c\left(1+\frac{y}{4}\right)\left[ln\left(\frac{1-b+x}{1+x}\right) + \sum_{k=1}^{3}\frac{b^k}{k(1+x)^k}\right] \tag{A.5}$$

where

$$y = \frac{E_\gamma^2}{E(E-E_\gamma)}, \qquad a = \frac{1+\mu_p^2}{4} + \frac{4m_p^2}{Q_0^2} \approx 7.16$$
$$b = 1 - \frac{4m_p^2}{Q_0^2} \approx -3.96, \qquad c = \frac{\mu_p^2 - 1}{b^4} \approx 0.028 \tag{A.6}$$

Here Q^2_{max} and Q^2_{min} are the upper and lower bounds of the integration. The contribution to the integral above $Q^2_{max} \approx 2\ GeV^2$ is negligible. Therefore during calculations we set $Q^2_{max} = 2\ GeV^2$.

---

[1] G. Belanger and F. Boudjema Phys. Lett. B 288, 201 (1992).

[2] G. Belanger and F. Boudjema Phys. Lett. B 288, 210 (1992).

[3] O. J. P. Eboli, M. C. Gonzalez-Garcia and S. F. Novaes, Nucl. Phys. **B411**, 381 (1994).

[4] G. Abbiendi *et al.* [OPAL Collaboration], Phys. Rev. D **70**, 032005 (2004) [hep-ex/0402021].

[5] A. Abulencia *et al.* (CDF Collaboration), Phys. Rev. Lett. **98**, 112001 (2007); arXiv:hep-ex/0611040.

[6] T. Aaltonen *et al.* (CDF Collaboration), Phys. Rev. Lett. **102**, 222002 (2009); arXiv:0902.2816 [hep-ex].

[7] T. Aaltonen *et al.* (CDF Collaboration), Phys. Rev. Lett. **102**, 242001 (2009); arXiv:0902.1271 [hep-ex].

[8] O. Kepka and C. Royon, Phys. Rev. D **78**, 073005 (2008); arXiv:0808.0322 [hep-ph].

[9] V.A. Khoze, A.D. Martin and M.G. Ryskin, Eur. Phys. J. C **23**, 311 (2002); arXiv:hep-ph/0111078.

[10] N. Schul and K. Piotrzkowski, Nucl. Phys. B, Proc. Suppl., **179**, 289 (2008); arXiv:0806.1097 [hep-ph].

[11] S. M. Lietti, A. A. Natale, C. G. Roldao and R. Rosenfeld, Phys. Lett. B **497**, 243 (2001); arXiv:hep-ph/0009289.

[12] E. Chapon, C. Royon and O. Kepka , Phys. Rev. D **81**, 074003 (2010); arXiv:0912.5161 [hep-ph].

[13] S. Atağ, S. C. İnan and İ. Şahin, Phys. Rev. D **80**, 075009 (2009); arXiv:0904.2687 [hep-ph].

[14] İ. Şahin and S. C. İnan, JHEP **09**, 069 (2009); arXiv:0907.3290 [hep-ph].

[15] S. Atağ, S. C. İnan and İ. Şahin, JHEP **09**, 042 (2010); arXiv:1005.4792 [hep-ph].

[16] S. C. İnan, Phys. Rev. D **81**, 115002 (2010); arXiv:1005.3432 [hep-ph].

[17] S. Atağ and A. A. Billur, JHEP **11**, 060 (2010); arXiv:1005.2841 [hep-ph].

[18] M.G. Albrow, T.D. Coughlin and J.R. Forshaw, Prog. Part. Nucl. Phys. **65**,149-184 (2010); arXiv:1006.1289 [hep-ph].

[19] İ. Şahin, and A. A. Billur, Phys. Rev. D **83**, 035011 (2011); arXiv:1101.4998 [hep-ph].

[20] İ. Şahin, and M. Koksal, JHEP **03**, 100 (2011); arXiv:1010.3434 [hep-ph].

[21] R. S. Gupta, Phys. Rev. D **85**, 014006 (2012) [arXiv:1111.3354 [hep-ph]].

[22] İ. Şahin, Phys. Rev. D **85**, 033002 (2012) [arXiv:1201.4364 [hep-ph]].

[23] V. M. Budnev, I. F. Ginzburg, G. V. Meledin and V. G. Serbo, Phys. Rep. **15**, 181 (1975).

[24] G. Baur *et al.*, Phys. Rep. **364**, 359 (2002).

[25] K. Piotrzkowski, Phys. Rev. D **63**, 071502 (2001) [hep-ex/0009065].

[26] X. Rouby, Ph.D. thesis, Universite catholique de Louvain [UCL-Thesis 135-2008, CMS TS-2009/004], 2008.

[27] J. de Favereau de Jeneret, V. Lemaitre, Y. Liu, S. Ovyn, T. Pierzchala, K. Piotrzkowski, X. Rouby, N. Schul and M. Vander Donckt, arXiv:0908.2020 [hep-ph].

[28] C. Royon *et al.* (RP220 Collaboration), arXiv:0706.1796 [physics.ins-det], *Proceedings for the DIS 2007 workshop, Munich, 2007.*

[29] M.G. Albrow *et al.* (FP420 R and D Collaboration), JINST **4**, T10001 (2009); arXiv:0806.0302 [hep-ex].

[30] V. Avati and K. Osterberg, Report No. CERN-TOTEM-NOTE-2005-002, 2006.

[31] A. D. Martin, W. J. Stirling, R. S. Thorne and G. Watt, Phys. Lett. B **652**, 292 (2007); arXiv:0706.0459 [hep-ph].

[32] T. Kaneko in *New Computing Techniques in Physics Research*, edited by D. Perret-Gallix, W. Wojcik (CNRS, Paris, 1990); MINAMI-TATEYA Group, KEK Report No. 92-19, 1993; F. Yuasa *et al.*, Prog. Theor. Phys. Suppl. **138**, 18 (2000).

[33] V.A. Khoze, A.D. Martin and M.G. Ryskin, Eur. Phys. J. C **24**, 459 (2002).

[34] T. Pierzchala and K. Piotrzkowski, Nucl. Phys. Proc. Suppl. **179-180**, 257 (2008) arXiv:0807.1121 [hep-ph].

[35] K. Nakamura et al. (Particle Data Group), J. Phys. G 37, 075021 (2010).

[36] O. J. P. Eboli, M. C. Gonzalez-Garcia and S. M. Lietti, Phys. Rev. D **69**, 095005 (2004) [hep-ph/0310141].

[37] S. Atağ and İ. Şahin, Phys. Rev. D **75**, 073003 (2007) [hep-ph/0703201 [HEP-PH]].

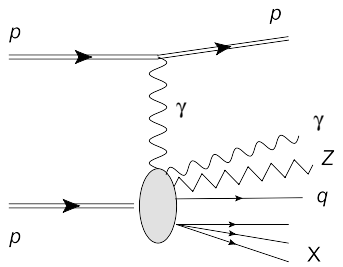

FIG. 1: Schematic diagram for the process $pp \to p\gamma p \to p\gamma qZX$.

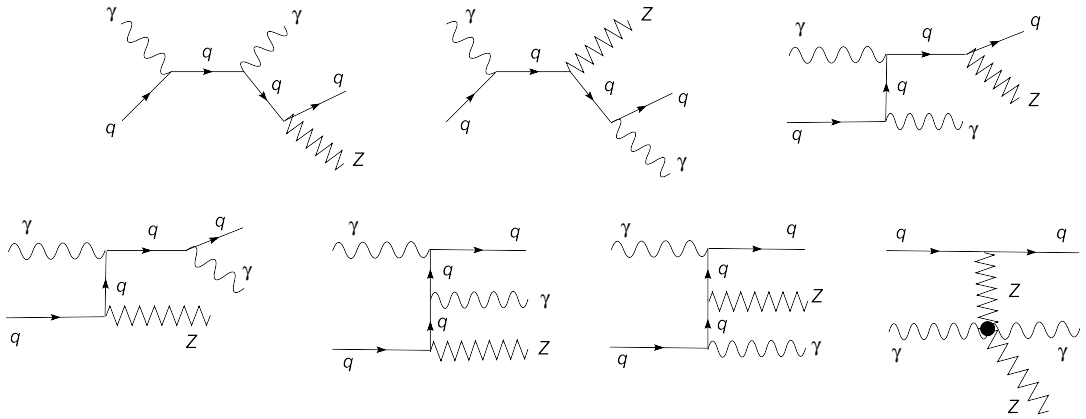

FIG. 2: Tree-level Feynman diagrams for the subprocess $\gamma q \to \gamma qZ$ ($q = u, d, c, s, b, \bar{u}, \bar{d}, \bar{c}, \bar{s}, \bar{b}$).

TABLE I: The number of observed events N_{obs} and corresponding values for upper limits N_{up} at 95% C.L. The calculated N_{obs} values are rounded to the nearest integer.

	$0.0015 < \xi < 0.5$		$0.0015 < \xi < 0.15$	
$L(fb^{-1})$	N_{obs}	N_{up}	N_{obs}	N_{up}
30	4	9.15	4	9.15
50	7	13.15	7	13.15
	$0.1 < \xi < 0.5$		$0.1 < \xi < 0.15$	
$L(fb^{-1})$	N_{obs}	N_{up}	N_{obs}	N_{up}
30	0	3.00	0	3.00
50	0	3.00	0	3.00
100	1	4.74	1	4.74
200	1	4.74	1	4.74

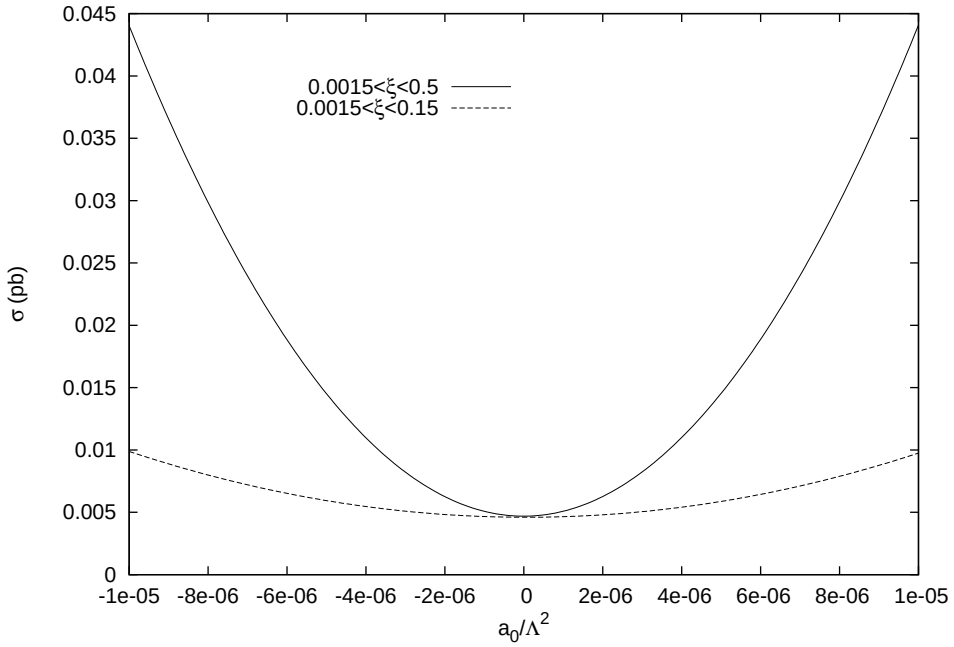

FIG. 3: Total cross section of $pp \to p\gamma p \to p\gamma qZX$ as a function of anomalous coupling $\frac{a_0}{\Lambda^2}$ for two different forward detector acceptances stated in the figure. The center-of-mass energy of the proton-proton system is taken to be $\sqrt{s} = 14$ TeV.

TABLE II: 95% C.L. sensitivity bounds of the couplings $\frac{a_0}{\Lambda^2}$ and $\frac{a_c}{\Lambda^2}$ for various LHC luminosities and forward detector acceptances of $0.0015 < \xi < 0.5$ and $0.1 < \xi < 0.5$. The center of mass energy of the proton-proton system is taken to be $\sqrt{s} = 14$ TeV.

	$0.0015 < \xi < 0.5$		$0.1 < \xi < 0.5$	
$L(fb^{-1})$	$\frac{a_0}{\Lambda^2}(\times 10^{-6}$ GeV$^{-2})$	$\frac{a_c}{\Lambda^2}(\times 10^{-6}$ GeV$^{-2})$	$\frac{a_0}{\Lambda^2}(\times 10^{-6}$ GeV$^{-2})$	$\frac{a_c}{\Lambda^2}(\times 10^{-6}$ GeV$^{-2})$
30	-4.0;4.0	-6.4;6.5	-2.8;2.8	-4.1;4.1
50	-3.4;3.4	-5.6;5.7	-2.2;2.2	-3.1;3.1
100	-2.5;2.5	-4.1;4.2	-1.9;1.9	-2.7;2.7
200	-2.1;2.1	-3.4;3.5	-1.2;1.2	-1.7;1.7

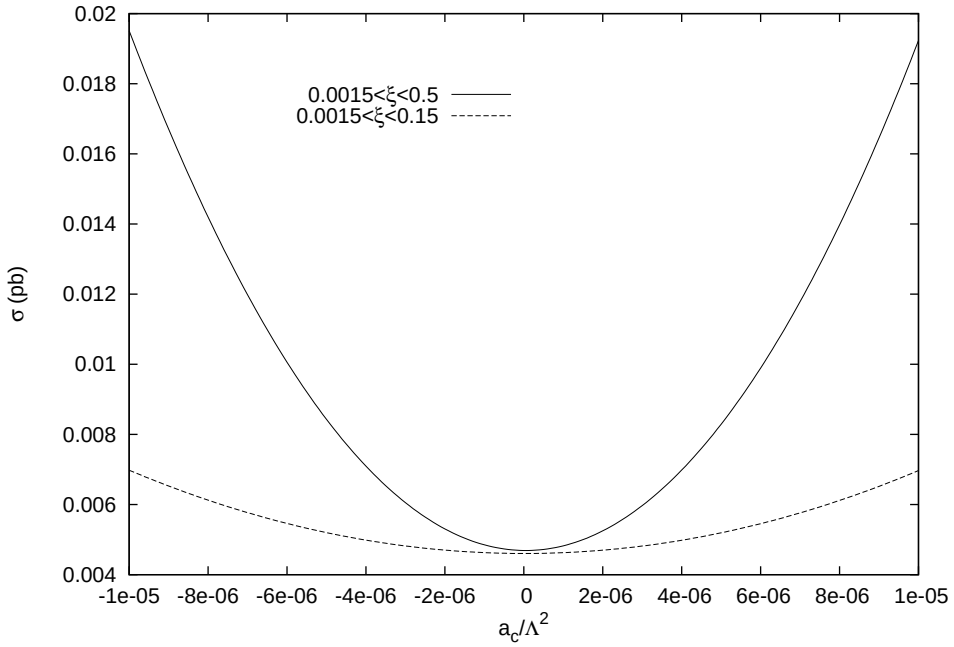

FIG. 4: Total cross section of $pp \to p\gamma p \to p\gamma qZX$ as a function of anomalous coupling $\frac{a_c}{\Lambda^2}$ for two different forward detector acceptances stated in the figure. The center-of-mass energy of the proton-proton system is taken to be $\sqrt{s} = 14$ TeV.

TABLE III: 95% C.L. sensitivity bounds of the couplings $\frac{a_0}{\Lambda^2}$ and $\frac{a_c}{\Lambda^2}$ for various LHC luminosities and forward detector acceptances of $0.0015 < \xi < 0.15$ and $0.1 < \xi < 0.15$. The center of mass energy of the proton-proton system is taken to be $\sqrt{s} = 14$ TeV.

	$0.0015 < \xi < 0.15$		$0.1 < \xi < 0.15$	
$L(fb^{-1})$	$\frac{a_0}{\Lambda^2}(\times 10^{-6}$ GeV$^{-2})$	$\frac{a_c}{\Lambda^2}(\times 10^{-6}$ GeV$^{-2})$	$\frac{a_0}{\Lambda^2}(\times 10^{-6}$ GeV$^{-2})$	$\frac{a_c}{\Lambda^2}(\times 10^{-6}$ GeV$^{-2})$
30	-10.9;11.0	-16.2;16.2	-9.5;9.5	-13.7;13.7
50	-9.5;9.6	-14.2;14.2	-7.3;7.3	-10.5;10.5
100	-6.9;7.0	-10.3;10.3	-6.4;6.4	-9.2;9.2
200	-5.8;5.9	-8.6;8.7	-4.3;4.3	-6.1;6.1